Development of a Quasi-static Model of NiMnGa Magnetic Shape Memory Alloy*

RONALD N. COUCH,† JAYANT SIROHI AND INDERJIT CHOPRA

Alfred Gessow Rotorcraft Center, Department of Aerospace Engineering, University of Maryland, College Park, USA

ABSTRACT: A quasi-static model for NiMnGa magnetic shape memory alloy is formulated along the lines of the Brinson and Tanaka SMA constitutive models. Since the shape memory effect (SME) and pseudoelasticity exist in both NiTi and NiMnGa, constitutive models for SMAs offer a basis for ferromagnetic shape memory alloys (FSMA) modeling. Two types of quasi-static tests involving constant external magnetic field and constant stress are conducted to identify nine model parameters. These model parameters include free strain, Young's moduli, fundamental critical stresses, fundamental critical threshold fields, and stress-influence coefficients. The Young's moduli of the material in its field and stress preferred states are determined to be 450 and 820 MPa respectively, while the free strain is measured to be 6.5%. These test data are used to assemble a critical stress–magnetic field intensity profile that is useful for determining the model parameters and for predicting the various states of the material for a wide range of magnetic or mechanical loading conditions. Although all of the parameters can be obtained from constant magnetic field testing, useful insight into NiMnGa actuator behavior can be gained from constant axial stress tests. Once implemented, the analytical model shows good correlation with the test data, capturing both the magnetic shape memory effect and pseudoelasticity. Because the model is piecewise linear, it does not capture material behavior resulting from nonlinear effects such as magnetic saturation. Despite its inherent limitations, this model shows encouraging results, providing a solid basis for future modeling efforts.

Key Words: magnetic shape memory, NiMnGa, martensite, quasi-static modeling, critical stress.

INTRODUCTION

FERROMAGNETIC shape memory alloys (FSMAs) show considerable potential as a viable actuator material. The FSMAs are suitable for many actuator applications that are currently closed to other active materials such as shape memory alloys (SMAs) and piezoelectrics because of limitations in either stroke or bandwidth. When a magnetic field in the order of 2 kOe is applied to the FSMA actuator, up to 10% plastic strain can be recovered, although 6–8% strain is more typical (O'Handley, 1998; Tellinen et al., 2002; Couch and Chopra, 2003; Mullner et al., 2003). One key advantage of magnetic SMAs is that its strain response has a wide bandwidth, reported to be well into the kHz range (Marioni et al., 2002; Couch and Chopra, 2003). In contrast, thermally driven SMAs like NiTi, have a very small bandwidth, not more than 1 Hz in ideal conditions due to the time involved with heating and cooling. Therefore, FSMAs have great potential for various applications requiring a high dynamic stroke.

One of the most widely known FSMAs, NiMnGa, can produce cyclic strains on the order of 6% and is a promising candidate for use in high stroke, smart actuators for a range of aerospace applications (Ulakko et al., 2000; Tellinen et al., 2002; Couch and Chopra, 2003). However, analytical tools are lacking at the present time and a comprehensive, constitutive model is required so that the behavior of the FSMA may be reliably predicted and the full engineering potential of this material may be utilized. At this time, a few micromechanical and thermodynamics based models are available, which predict the stress and strain states of NiMnGa in magnetic fields of up to 1.0 T (Likhachev and Ullakko, 2000; Murray, 2001; Mullner et al., 2002; Likhachev et al., 2004). From an engineering perspective, these models are not easy to implement, unlike the macromechanical constitutive models of NiTi (thermal SMA). Several of these constitutive models, supported by experimental data, have been formulated for SMAs including the models by Tanaka (1986), Rogers and Liang (1990), Brinson (1993) and Prahlad and Chopra (2001). Since they rely on experimentally

†Author to whom correspondence should be addressed.
E-mail: rncouch@eng.umd.edu
*'This paper was originally presented at the Fifteenth International Conference on Adaptive Structures and Technologies (2004 ICAST)'.
Figures 2 and 4–12 appear in color online: http://jim.sagepub.com

1045-389X/07/06 0611–12 $10.00/0 DOI: 10.1177/1045389X06067930

determined material parameters, these models are easy to implement and serve as an important ingredient toward the development of intelligent systems. A macromechanical constitutive model, similar to those used to model NiTi, is required for NiMnGa. The subject of this study is the initial development of a phenomenological-based global model, characterized by test data, developed along the lines of the Brinson model. The key issue to resolve with this approach is that the NiTi-based model must be modified to accommodate strains induced by a magnetic field instead of a thermal field.

Tests are directed toward determining the model parameters for NiMnGa rods subjected to quasi-static, uniaxial loading conditions. There are nine parameters that must be determined including threshold fields, fundamental critical stresses, Young's moduli in the stress and field preferred martensite states, stress-influence coefficients, and free strain. Since these constants are functions of the applied magnetic field and applied axial stress, the NiMnGa rods are tested under a wide range of magnetic and mechanical loading conditions. A series of uniaxial compression tests of the NiMnGa subjected to both constant applied magnetic field intensities and constant stress were conducted to determine each of the nine parameters. Once the parameters were identified, the model was implemented and compared with experimental data, fostering a discussion regarding the validity of the model.

BACKGROUND

NiMnGa is a relatively new active material, first discovered by O'Handley (1996) and then by Ullakko et al. (1996). Its ability to produce large strains in the order of 6% at frequencies well into the kHz range have made it an attractive candidate for many applications, especially those involving high stroke and low force requirements (Tellinen et al., 2002; Marioni et al., 2002; Mullner et al., 2003). The FSMAs are a unique category of shape memory materials because they exhibit shape memory properties when the material is in the low temperature phase. Unlike conventional shape memory materials, like NiTi, which rely on heating and cooling processes for strain recovery, NiMnGa operates by the mechanism of magnetically induced twin boundary motion. Because NiMnGa does not depend on a phase change to recover strain, it can be operated at much higher frequencies (>1 kHz) than its thermally driven counterparts.

Strain Recovery Mechanism in NiMnGa

The magnetically induced strains in NiMnGa are a direct result of the rearrangement of the martensite twin structure of the material (Ulakko et al., 1996, 2000; Sovinov et al., 2002; Couch and Chopra, 2003; Mullner et al., 2003). At the high temperature austenite state, NiMnGa has a cubic lattice unit cell structure. When cooled to the martensite phase, the unit cell reverts to a tetragonal configuration consisting of a long axis (*a*-axis) and a short axis (*c*-axis). Furthermore, this martensite phase is subdivided into two primary variants: a field preferred and a stress preferred. The *c*-axis is aligned parallel to the axis of magnetization, also known as the 'easy' axis. Like any ferromagnetic material, the axis of magnetization will align itself with the direction of an external field. In magnetic SMAs like NiMnGa, this process is not easily accomplished because the material exhibits a high degree of magnetocrystalline anisotropy. The effect of this anisotropy is to rigidly fix the axis of magnetization within the unit cell along the *c*-axis. Therefore, when an external field is applied to the actuator, the entire unit cell itself, tends to rotate to align the easy axis with the field direction. This process of unit cell realignment causes the material to grow field-preferred twin variants at the expense of stress-preferred variants. As the NiMnGa specimen transitions from a stress-preferred to field-preferred state, a change in dimension is observed. This change in actuator dimension is known as the magnetic shape memory effect (MSME). The magnitude of the induced strain depends on factors such as chemical composition, thermomechanical history, and heat treatment (Cheng et al., 2004).

For bar-shaped NiMnGa actuators, an external magnetic field induces axial strain perpendicular to the direction of the applied field. The induced strain may be recovered by applying an axial, compressive stress to the actuator along the direction of strain. Hence, the material is described as having two states, a field-preferred state and a stress-preferred state. When an FSMA in the stress-preferred state is exposed to a sufficient magnetic field at zero stress, twin boundary motion will occur causing the actuator to become 'detwinned' martensite and achieve its free strain of ~6%. This state is known as the field-preferred state. After an axial compressive load in the order of 3–4 MPa has been applied to the rod at zero applied field, the twins are reordered and the actuator converts to a fully twinned or stress-preferred state.

The FSMAs, like NiMnGa, exhibit strain recovery phenomena similar to conventional, thermally driven SMAs, such as NiTi. Both materials exhibit the shape memory effect (SME) and pseudoelastic behavior. The obvious difference between the two materials is that NiTi requires a thermal field and NiMnGa requires a magnetic field for actuation. The MSME may be observed by applying an external field to a NiMnGa actuator initially in the stress-preferred state to induce twin boundary motion and transform the actuator to the

field-preferred state. With the external field removed, the resulting strain can be recovered by applying an axial stress of at least 3 MPa. An external field of at least 2 kOe applied after the stress is removed induces twin boundary motion in the actuator, reverting the specimen back to its field-preferred state, and reintroducing magnetically induced strain into the sample. This MSME is shown schematically in Figure 1(a). NiMnGa also exhibits pseudoelastic behavior. When the material, initially in the field-preferred state, is subjected to increasing, axial, compressive stress while exposed to a large magnetic field in the order of 4 kOe, the actuator will undergo a transformation from field-to stress-preferred martensite, inducing a large plastic strain. Upon the removal of stress, the strain is completely recovered in a hysteresis loop. Figure 1(b) shows a schematic of the concept of magnetic pseudo-elasticity in FSMAs.

It is important to note that these strain recovery mechanisms are only present when the material is in the low temperature, martensite phase. As a result, care must be taken to ensure that the material operates in a low temperature environment. For NiMnGa, the martensite to austenite transformation temperature occurs at 56°C, well above room temperature (Couch and Chopra, 2003). Regarding the present work, all tests were conducted at room temperature (25°C) to ensure that the actuator was completely in the martensite phase and that all induced strains observed are assumed to be the result of the MSME or magnetic pseudoelasticity.

Quasi-static Modeling of FSMA Actuators

Because of the close similarities that exist between the behavior of NiTi and NiMnGa, it is possible to assume that existing phenomenological models for NiTi can provide a basis for FSMA modeling. There are several constitutive models that are used to predict the stress–strain behavior of thermally activated SMAs. The models of Tanaka (1986), Liang and Rogers (1990), and Brinson (1993) are all based on experimentally determined material parameters. All three models are quite similar, describing the material behavior in terms of three state variables namely, stress, strain, and temperature. Because Brinson's is the most comprehensive of the three models, it will be used as a basis for developing a quasi-static FSMA model.

The constitutive equation for the Brinson model using constant material functions is,

$$\begin{aligned}\sigma - \sigma_0 = {} & E(\xi)(\varepsilon - \varepsilon_0) + \Omega_s(\xi_s - \xi_{s0}) \\ & + \Omega_T(\xi_T - \xi_{T0}) + \theta(T - T_0)\end{aligned} \tag{1}$$

where E is the Young's modulus as a function of the martensite volume fraction, ξ, Ω_s and Ω_T are stress and temperature induced transformation tensors respectively, and θ is related to the thermal coefficient of expansion. The initial conditions, σ_0, ε_0, ξ_{s0}, ξ_{T0}, and T_0, are included. Similarly, the proposed NiMnGa quasi-static behavioral model takes the following form,

$$\begin{aligned}\sigma - \sigma_0 = {} & E(\xi_\sigma)(\varepsilon - \varepsilon_0) + \Omega(\xi_\sigma)(\xi_\sigma - \xi_{\sigma 0}) \\ & + \lambda(\xi_{\sigma 0})(H - H_0)\end{aligned} \tag{2}$$

where σ_0, ε_0, $\xi_{\sigma 0}$, and H_0 represent the initial stress, strain, volume fraction of stress preferred martensite, and magnetic field intensity respectively. E, Ω, and λ are constant material functions where E represents the Young's modulus of the FSMA, Ω is a transformation tensor, and λ is related to the magnetostriction of the material. Each of these material functions are defined in relation to the volume fraction of the stress-preferred martensite, ξ_σ. A magnetic field applied to the FSMA causes the volume fraction of the stress-preferred martensite to decrease resulting in the growth of field-preferred martensite twins. This is analogous to the phase transition from martensite to austenite in NiTi SMA. However, as previously mentioned, strain recovery in NiTi SMA occurs as a result of a phase transformation, while in FSMA strain recovery occurs as a result of twin boundary motion in the martensite

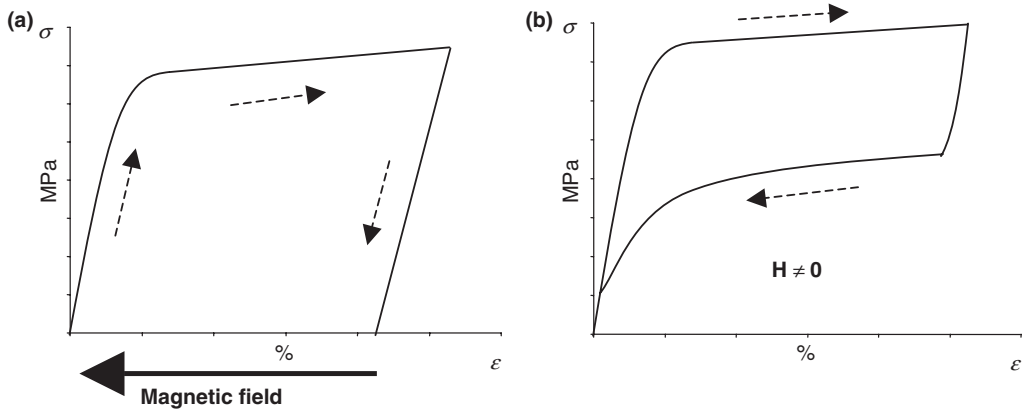

Figure 1. *(a) Schematic representation of the MSME at zero initial applied field and (b) magnetic pseudoelasticity in the presence of a large external field.*

phase only. Therefore, the sum of the stress-preferred martensite, ξ_σ, and field-preferred martensite ξ_H must always be equal to unity.

$$\xi_\sigma + \xi_H = 1. \tag{3}$$

If it is assumed that the material is at the maximum free-strain condition, $\varepsilon = \varepsilon_L$, with the material initially composed entirely of the field-preferred variant, $\xi_{\sigma 0} = 0$, with the initial conditions of $\sigma_0 = \varepsilon_0 = H_0 = 0$, and final conditions of $\xi_\sigma = 1$, $\varepsilon = \varepsilon_L$, and $\sigma = H = 0$, the following relation can be obtained:

$$\Omega = -\varepsilon_L E. \tag{4}$$

Using the constraint derived in Equation (4), the FSMA constitutive equation may be reduced to the following simplified form,

$$\sigma = E(\xi_\sigma)(\varepsilon - \varepsilon_L \xi_\sigma) + \lambda(\xi_\sigma)(H - H_0), \tag{5}$$

where $E(\xi_\sigma)$ is the Young's modulus of the material as a function of the stress-preferred martensite volume fraction, ε_L is the free-strain of the actuator, ξ_s is the stress-preferred volume fraction, λ is related to the magnetostriction of the material and H_0 is the initial external field applied to the material.

The phenomenological model for NiMnGa describes the state of the material in terms of three state variables: stress, strain, and magnetic field. The model is characterized by nine experimentally determined constants. The nine model constants include: three material parameters: free strain, ε_L, stress-preferred martensite Young's modulus, E_σ, field-preferred martensite Young's modulus, E_H; two fundamental threshold fields: H_s, H_f; two stress-influence coefficients: C_s, and C_f; and two fundamental critical stresses: $\sigma_{cr,s}$ and $\sigma_{cr,f}$. These nine constants are directly analogous to the parameters defined in the Brinson formulation. In Table 1 the parameters defined in the FSMA model and their Brinson model counterparts are shown. Free strain and Young's moduli can be determined from stress–strain curves for the actuator exposed to a constant external field. The remaining six constants can be determined from a profile of critical stresses as a function of applied field intensity. This profile may be generated from either constant stress or constant field tests but it will be shown that a profile generated from constant field testing is the more reliable of the two methods.

EXPERIMENTAL SETUP

The two single crystal, martensite, NiMnGa rods used in this study were obtained from Adaptamat (Finland). The specimen dimensions were $2 \times 3 \times 16$ mm. In addition, the magnetic easy, or c-axis, is oriented parallel to the direction of the long axis. Therefore, magnetic strain is induced when a field is applied perpendicular to the long axis of the NiMnGa Rod. Each single crystal specimen was oriented and cut by the manufacturer to produce this type of motion. Upon delivery, each specimen was magnetically cycled a few times (20–30 times) before experiments were conducted in order to relieve any internal stresses incurred during the manufacturing process. The density of the material was measured to be 8.36 g/cm^3.

To determine the necessary constants for the model, two types of tests were conducted, a constant stress test and a constant applied magnetic field test. Each of the tests was carried out in separate test rigs, built inhouse. Both test rigs were designed around similar electromagnetic circuits. The DC magnetic fields were applied by a laminated, transformer-steel core electromagnet capable of producing field intensities in the order of 10 kOe. The cores were divided into two E-shaped halves, each consisting of a series of transformer steel layers. The halves were joined together by an aluminum frame and an air gap was machined out of the center bars of the E-frame to create magnetic poles. Two, 500 turn, copper wire coils, connected in parallel were fixed to the poles of the laminated core by interchangeable Delrin bobbins. The NiMnGa specimen was situated in between the two tapered poles of the electromagnet where a uniform, transverse field could be applied to the entire specimen. An air gap of $\sim$0.020 in. existed between the NiMnGa specimen and the two pole faces.

To ensure that a proper field distribution was applied along the length of the specimen, Hall effect sensors

Table 1. List of FSMA model parameters and their Brinson model counterparts.

FSMA model parameter	Symbol	Symbol	Brinson model parameter
Free strain	ε_L	ε_L	Maximum residual strain
Stress preferred Young's modulus	E_σ	E_A	Young's modulus: austenite
Field preferred Young's modulus	E_H	E_M	Young's modulus: martensite
Zero stress threshold field start	H_s	A_s	Austenite start temperature (zero stress)
Zero stress threshold field finish	H_f	A_f	Austenite finish temperature (zero stress)
Stress influence coefficient (start)	C_s	C_M	Stress influence coefficient (martensite)
Stress influence coefficient (finish)	C_f	C_A	Stress influence coefficient (austenite)
Zero field critical stress start	$\sigma_{cr,s}$	$\sigma^{cr}{}_s$	Critical stress start (martensite)
Zero field critical stress finish	$\sigma_{cr,f}$	$\sigma^{cr}{}_f$	Critical stress finish (martensite)

were used to characterize the uniformity of the field between the poles. The sensors were placed at regularly spaced intervals along the length of the NiMnGa actuator so that a profile of the field applied to the actuator could be developed. Based on this profile, the applied magnetic field varied less than 2% along the plane of the pole face and was therefore assumed to be uniform for the purpose of these tests.

Constant Magnetic Field Testing Apparatus

For the constant applied magnetic field tests, the NiMnGa specimen was gripped between a 10 lb load cell and a moveable carriage. To ensure that the specimen was entirely exposed to the uniform field, it was carefully situated within the air gap in the magnetic circuit. The carriage was driven by a screw and a NEMA-23 precision stepper motor assembly. Axial loads were applied to the specimen by energizing the stepper motor and allowing it to compress the FSMA rod against the load cell at a prescribed strain rate. To maintain a quasi-static condition, the specimen was compressed at a rate of 0.02 mm/s. The accuracy of the load cell was within 0.0045 N. Actuator strain was determined by measuring the angular deflection of the motor with a potentiometer. The accuracy of the strain measurement was within 0.01 mm. The magnetic field, B, was measured by a Hall sensor placed in the air gap between the specimen and pole face. The field intensity, H, generated by the coils, was determined by calibrating the electromagnet with the level of current in the coils. The coil current was determined by measuring the voltage across a 1 Ω precision resistor connected in series between the coil and ground. The electromagnet was powered by two 30 V/10 A DC power supplies. A photograph of the constant field test rig is shown in Figure 2.

Constant Axial Stress Testing Apparatus

Constant stress tests were carried out on a rig similar to that used in the constant applied field tests. The main difference between the two rigs is that the specimen is oriented horizontally in the constant applied field test and vertically in the constant stress test. The NiMnGa specimen was glued into grips between the poles of the electromagnet. Special care was taken to ensure that small amounts of high shear stiffness, low viscosity, cyanoacrylate adhesive were used to bond the specimen with the grip. This was carried out to minimize the effect of the bond layer on the twin boundary motion of the NiMnGa. The specimen was supported by a stationary, lower rod so that strain was restricted to one direction. In the direction of strain, the specimen acted against a rod attached to a low-friction linear bearing. Another rod at the other end of the bearing connected the bearing–pushrod combination to a linear potentiometer and weight pan. Strains were measured by the linear potentiometer, accurate to within 0.002 mm, and the level of constant stress was regulated by adding and subtracting weights from the weight pan. Magnetic field measurements were taken by Hall effect sensors located in the air gap between the pole and NiMnGa bar. The electromagnet in this rig was powered by two 30 V/5 A power supplies connected in series, and a rack of capacitors connected in parallel with the coils for use when the power supplies were turned off. These capacitors provided the high RC constant which is necessary to have a slow decay in the magnetic field when the power was removed. This was carried out so that the quasi-static behavior of the material could be observed. A photograph of the constant stress test rig is shown in Figure 3.

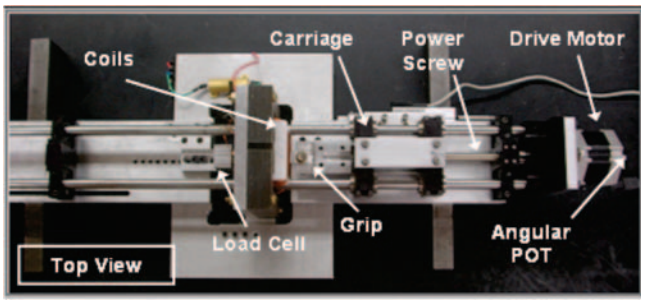

Figure 2. *Constant applied magnetic field testing apparatus.*

EXPERIMENTAL PROCEDURE

The first category of testing, the constant stress tests, involved magnetically cycling the NiMnGa actuator while it was exposed to a constant axial stress field. First, an axial stress of 3 MPa was applied to and removed from the specimen to ensure that the actuator was initially in the stress-preferred state. Next, the weights were added to the weight pan until the desired constant stress level was reached. The coils were then energized and the magnetic field was allowed to vary quasi-statically from 0 to 1.1 T. Halfway through the test, the power to the coils was removed and the field was allowed to decay slowly, at the rate prescribed by the RC constant of the capacitors discharging through the coils. As in the constant applied field tests, time histories of the magnetic field and the actuator displacement were recorded over the entire test duration.

The second type of test involved observing the specimen under constant, applied magnetic fields. These tests were conducted by energizing the NiMnGa rod with a uniform, external magnetic field and then varying the level of compressive stress applied to the

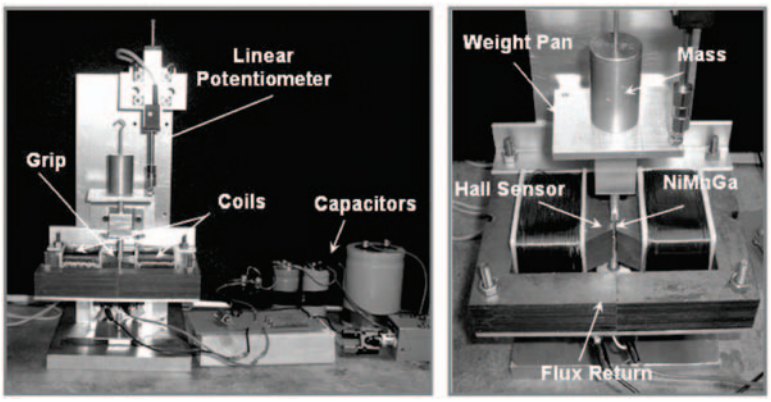

Figure 3. *Constant axial stress testing apparatus.*

rod. First, the specimen was magnetically cycled from 0 to 8 kOe, at zero stress to induce the MSME, thereby ensuring that the material is initially in the field-preferred state. Then, a precision stepper motor was used to quasi-statically compress the specimen to a stress level of 5–6 MPa. This stress level is sufficient to completely convert the NiMnGa to the stress-preferred variant. The load was then removed quasi-statically while still under the influence of the external field. The NiMnGa rod was mechanically cycled in this manner, while exposed to various levels of constant external field intensities ranging from 0 to 12 kOe. Time histories of the load, strain, and inductive field were recorded by the data acquisition system.

RESULTS AND DISCUSSION

The parameters necessary for characterization of the quasi-static model were obtained from experiments involving the variation of stress in a constant applied field environment and the variation of magnetic field (inductive) in a constant stress environment. Because each test was conducted quasi-statically, dynamic effects are not included. Once the constants were obtained, the model was implemented and compared to the experimental data. Limitations of the model are also identified and discussed.

Constant Axial Stress Testing

Constant stress testing provides a direct measurement of the actuation capabilities and threshold fields of the material for different loads. For thermal SMAs, constant stress testing is used to develop a profile of the critical stress versus temperature behavior of the material (Prahlad and Chopra, 2001). This profile can then be used to determine the remaining constants of the model as well as predict the state of the material for any set of loading conditions. Likewise for NiMnGa, a similar profile will be developed. In these tests, the strain behavior of the material was observed by applying a constant stress to the actuator while the material was subjected to a time varying magnetic field of up to 1.1 T. Figure 4(a) and (b) shows typical results from these tests.

In Figure 4(a), the material behavior acting against a constant stress of 0.4 MPa is shown. As the field is increased, the FSMA begins to convert from stress-preferred to field-preferred martensite at 0.24 T. The actuator completes this transformation to the field-preferred state at 0.68 T. These threshold fields represent the start and finish of the detwinning behavior for this constant stress level. Over the course of this transformation, the actuator undergoes 6.5% strain. When the field is removed, the actuator begins to revert back to the stress-preferred state at 0.55 T. This field represents the threshold of the reverse transition from field- to stress-preferred martensite. But when the field returns to zero, the magnitude of constant stress is not sufficient to entirely compress the actuator back to its fully twinned condition. As a result, a residual strain remains. This residual strain may be removed by applying additional axial force to the actuator. For cases where low axial stress is applied to the NiMnGa, only two or three critical fields may be detected.

In Figure 4(b), the specimen is acting against a constant stress of 1.3 MPa. At this stress level, the threshold fields for the transition from the stress- to the field-preferred variant are 0.42 T and 0.88 T respectively, substantially higher than those for the 0.4 MPa axial stress case. Likewise, the critical fields for the reverse transition are also higher (0.61 and 0.12 T). At 1.3 MPa, there is no residual strain when the field returns to zero because the axial stress is sufficient to induce the fully twinned, stress-preferred state in the material. For instances where a large axial stress is applied to the rod, all four critical threshold fields may be determined.

There is one primary drawback to this type of testing. For low stress levels, the critical threshold fields are

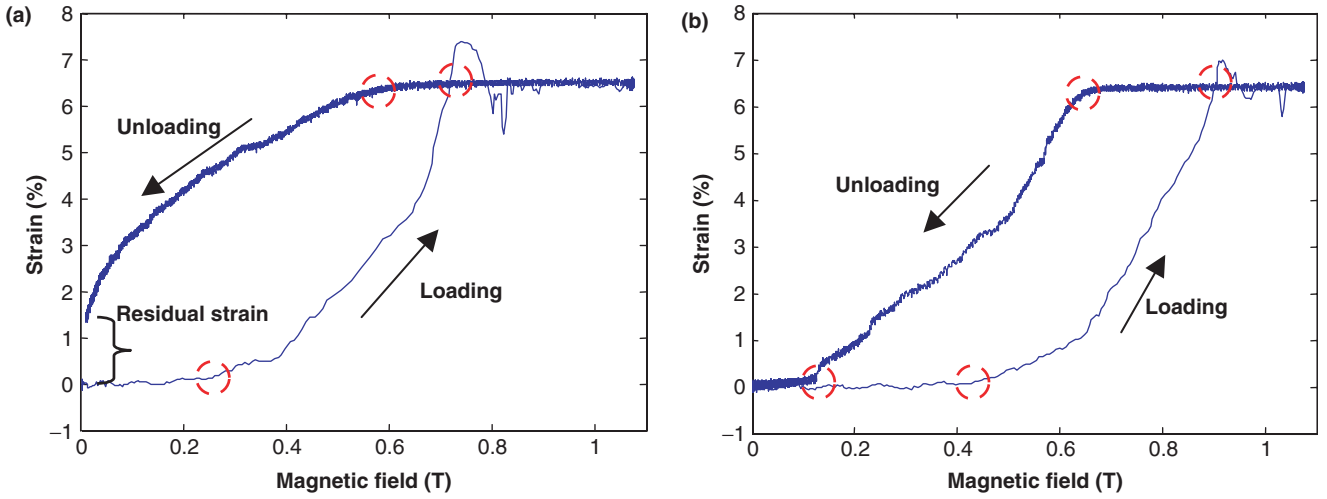

Figure 4. *Constant stress test results: (a) 0.4 MPa and (b) 1.3 MPa.*

less distinct which can lead to errors in determining precisely, the fields that induce twin boundary motion. Consider the case of 0.4 MPa of constant stress in Figure 4(a). It can be argued that while the threshold fields for the transition from stress- to field-preferred variants during magnetic loading are distinct, the same cannot be said for the reverse transition when the field is removed. Because there appears to be a smooth transition between the twin variants at this loading, it is difficult to determine distinct points indicating the beginning of the twin boundary motion. This can lead to substantial uncertainty in the identification of the threshold fields. Therefore, while constant stress testing is useful for model characterization of SMA behavior, it may not be the most consistent approach for obtaining the FSMA model parameters.

Constant stress testing is most useful in providing insight into the maximum strain capability of the actuator material as well as the phenomenon of residual strain. In Figure 5, the maximum strain and residual strain as functions of constant stress are shown. For applied stress below 2 MPa, the maximum strain remains at a level of ~6.5%. At higher stresses, the maximum achievable strain decreases in a sharply linear fashion. This behavior is not a property of the material but occurs due to the lack of magnetic field. For stresses above 2.0 MPa, the maximum applied field of 1.1 T is not strong enough to overcome the load and completely convert the actuator to field-preferred martensite. Based on this trend, the actuator will be blocked at 2.75 MPa for the 1.1 T applied field. In Figure 5(b), the residual strain as a function of stress is shown. The residual strain remains at ~6.3% until a stress of 0.3 MPa is applied. Beyond this stress level, the strain falls off rapidly until 0.73 MPa, and at which point the residual strain becomes zero. At this point, the actuator is fully reverted to stress-preferred martensite upon removal of the field. The existence of a residual strain indicates that the material is in an intermediate state, composed of both stress- and field-preferred variants. Considering both plots, the total stroke of the FSMA element, under a constant stress field for one cycle of magnetic loading is equal to the difference between twice the maximum strain predicted in Figure 5(a) and the residual strain predicted in Figure 5(b).

Constant Applied Field Testing

The NiMnGa actuator was tested at constant field intensities ranging from 0 to 12 kOe. Figure 6 shows stress–strain curves resulting from these tests. These constant applied field tests were highly repeatable, showing little variation between successive loading cycles. In each case, the material behaves according to the same fundamental pattern. First, the NiMnGa actuator begins in the field-preferred variant and as the compressive stress is quasi-statically applied from 0 to 6 MPa, the strain is initially linearly related to stress until a critical stress level is reached. The stiffness of the material in this region, E_H, is the stiffness of the field-preferred martensite variant of NiMnGa. Above this first critical stress level, σ_1, the material undergoes a rapid decrease in stiffness accompanied by a large increase in strain. In this region, twin boundary motion is induced and the material converts from the field- to the stress-preferred martensite variant. This behavior will continue until the material reaches a second critical stress, σ_2. Above this stress, the material has a volume fraction of stress-preferred martensite equal to 1.0 and the stiffness increases sharply to E_σ, which is the stiffness of the stress-preferred variant. When the load is removed from the material, similar parameters can be identified for the reverse transition from the stress- to the

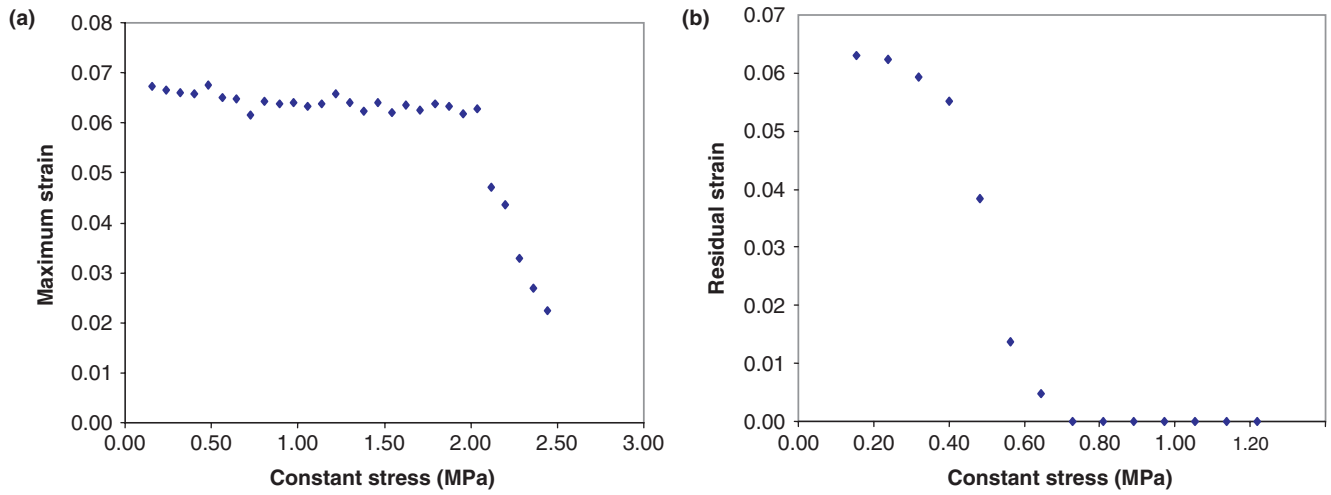

Figure 5. *NiMnGa actuator subjected to constant axial stress: (a) maximum strain induced by 7.5 kOe field and (b) residual strain.*

field-preferred variant. Figure 6(a) shows these parameters for the case of a 6 kOe external field. The Young's modulus for the field preferred variant, E_H, was determined to be 450 MPa, while the Young's modulus for the stress-preferred variant, E_σ was determined to be 820 MPa. In Figure 6(b) the effect of increasing the applied field on the stress–strain behavior of the material is shown. The slope of the stress–strain curve before Φ_1 is unaffected by increasing the field intensity and likewise, the slope of the stress–strain curves above Φ_2 is similarly unaffected. As a result, it can be concluded that the moduli of the field-preferred variant (below Φ_1) and the stress-preferred variant (above Φ_2) are unaffected by the magnitude of the external field intensity. Clearly, the main effect of increasing the field intensity is to raise the level of the critical stresses that signify the start and finish of the twin boundary motion. Figure 6(b) also illustrates the magnetic pseudoelastic effect. For each applied field, the material completely recovers the strain in a hysteresis loop as the axial stress is removed.

Identification of the critical stresses for a range of field intensities enables the development of a critical stress profile (Figure 7). The critical stresses that define the twin boundary motion for the FSMA actuator during loading are denoted as σ_1 and σ_2; the beginning and end of the transition, respectively. For twin boundary motion during unloading, σ_3 and σ_4 are similarly defined. Each curve of the critical stress behavior follows a linear path for fields below 7 kOe. For fields larger than 7 kOe, the critical stresses begin to level off, indicating the onset of magnetic saturation. Because the σ_1 and σ_3 curves are coincident and the σ_2 and σ_4 curves are parallel, it is sufficient to define two stress influence coefficients. The first stress influence coefficient, C_s, is defined as the slope of the σ_1 and σ_3 curves, or in other words, the variation of critical stress with applied field for the onset of twin boundary motion. The second stress influence coefficient representing the critical stress behavior at the conclusion of twin boundary motion, C_f, is determined from the slope of the σ_2 and σ_4 curves. Since this is a linear model, higher-order effects like magnetic saturation, are neglected. Each coefficient has units of MPa/kOe. Based on experimental data, a C_s of 0.452 MPa/kOe and a C_f of 0.488 MPa/kOe were determined.

The critical stress profile also contains two other features that lead to model parameters. First, the points corresponding with zero applied field of the σ_1 and σ_2 curves are the two fundamental critical stresses $\sigma_{cr,s}$ and $\sigma_{cr,f}$. Along with the appropriate stress influence coefficients, these parameters can be used to predict the critical stresses for any applied field during the loading cycle. These fundamental critical stresses are 0.284 MPa and 0.920 MPa for $\sigma_{cr,s}$ and $\sigma_{cr,f}$ respectively. The critical stresses of the reverse transition, σ_3 and σ_4, exist only above certain threshold fields. By noting the x-intercepts of these two curves, the two fundamental, zero stress threshold fields may be identified. For instance, the x-intercept of the σ_3 curve is 1.0 kOe. For external field intensities greater than 1.0 kOe, the actuator will begin to revert to the field preferred state when the load is removed. This field is the H_s parameter of the model. Likewise, the H_f field may be defined by the x-intercept of the σ_4 curve, which is 3.5 kOe. Critical stresses for the unloading portion of the mechanical cycle may be determined from these critical fields as well as the stress influence coefficients. It must also be pointed out that a partial magnetic pseudoelastic effect occurs for applied fields between H_s and H_f while complete magnetic pseudoelasticity occurs for fields greater than or equal to H_f. In the partial pseudoelastic region, the strain does not return to zero upon removal of the load. In Figure 8, the zero-field behavior (MSME), the partial pseudoelastic

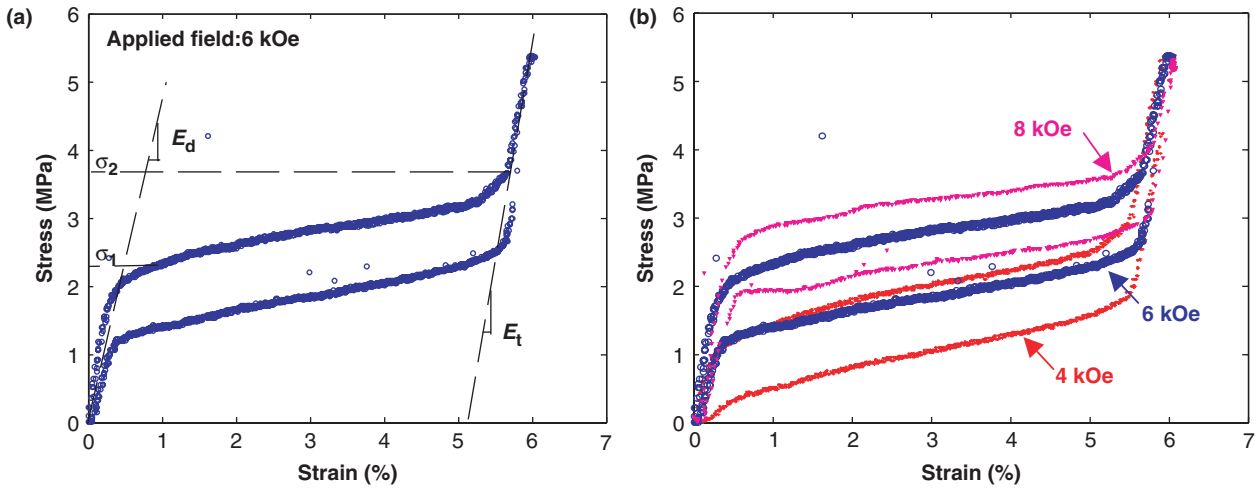

Figure 6. *Effect of constant magnetic field on the stress–strain behavior of NiMnGa: (a) material parameters at 6 kOe and (b) effect of increasing field on NiMnGa behavior.*

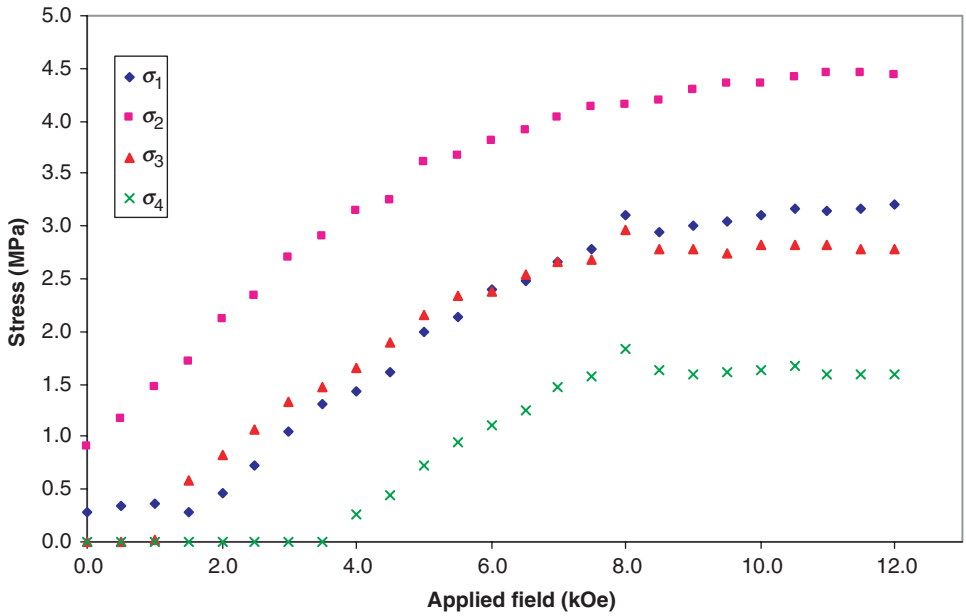

Figure 7. *Critical stress-magnetic field intensity profile for NiMnGa.*

effect at 2 kOe, and the complete pseudoelastic effect at 6 kOe are shown.

The final model parameter to be determined is the free strain, ε_L. The free strain is defined as the maximum recoverable plastic strain that can be recovered with the application of a sufficient magnetic field. This parameter may be determined by considering the stress–strain curve of NiMnGa for zero applied field shown in Figure 9. Because there is no applied field acting upon the FSMA, there will be no MSME induced strain recovery when the load is removed. When the stress is reduced to zero, the actuator recovers a small amount of elastic strain. The remaining strain is plastic in nature but can be recovered when a sufficient external field is applied at zero stress. The magnitude of the plastic strain, 5.5%, is the ε_L parameter of the quasi-static model.

FSMA Quasi-static Model

Once the model parameters are identified, the quasi-static model was implemented and validated with experimental data. The model calculates the stress in the actuator for a discrete number of strain steps. Once the stress reaches a critical value, twin boundary motion occurs. These critical stresses are functions of applied magnetic field and can be determined from the corresponding combination of parameters $\sigma_{cr,s}$, $\sigma_{cr,f}$, C_s, C_f, H_s, and H_f. In addition, a linear function is used to describe the transformation from stress- to

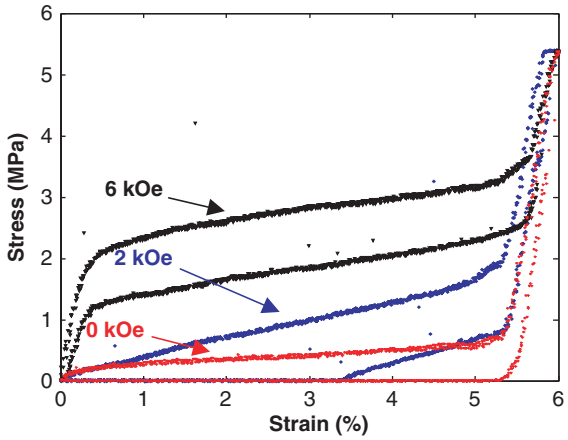

Figure 8. Magnetic shape memory (0 kOe), partial pseudoelasticity (2 kOe), and the pseudoelastic effect (6 kOe) of NiMnGa.

field-preferred martensite. A summary of the material parameters used in the model is shown in Table 2. In general, the model shows good agreement with the experimental data. Since the model is able to capture both SME and magnetic pseudoelasticity, it successfully exceeds the first benchmark. The model does not, however, capture the smooth transitions between the twinned and detwinned martensite states, therefore over-predicting the stresses in the material near the critical stresses of the loading cycle. For this same reason, the model tends to under-predict the material stresses during the unloading cycle.

The first benchmark for a successful NiMnGa behavioral model is that it must be able to capture both MSME and pseudoelasticity. In Figure 10(a), the result from the analytical model is compared to the experimental stress–strain curve for the zero field condition to show the model's effectiveness at capturing the MSME. Figure 10(b) shows the results of the model compared to the stress–strain curve for a specimen exposed to a constant 6 kOe field, to show the model's ability to capture magnetic pseudoelastic behavior.

In general, the model shows good agreement with the experimental data. Since the model is able to capture both SME and magnetic pseudoelasticity, it successfully exceeds the first benchmark. The model does not, however, capture the smooth transitions between the twinned and detwinned martensite states, therefore over-predicting the stresses in the material near the critical stresses of the loading cycle. For the same reason, the model tends to under-predict the material stresses during the unloading cycle.

Currently, the analytical model has some limitations and hence requires further refinement. One of the underlying assumptions of the model is that all the parameters are constant coefficients, effectively linearizing the model. As a result, higher-order effects, such as magnetic saturation, are not reflected in the predicted stress–strain curves. This means that

Table 2. Experimentally determined FSMA quasi-static model parameters.

Parameter	Value	Units
H_s	1.0	kOe
H_f	3.5	kOe
$\sigma_{cr,s}$	0.284	MPa
$\sigma_{cr,f}$	0.902	MPa
C_s	0.452	MPa/kOe
C_f	0.488	MPa/kOe
E_σ	820	MPa
E_H	450	MPa
ε_L	5.5	%

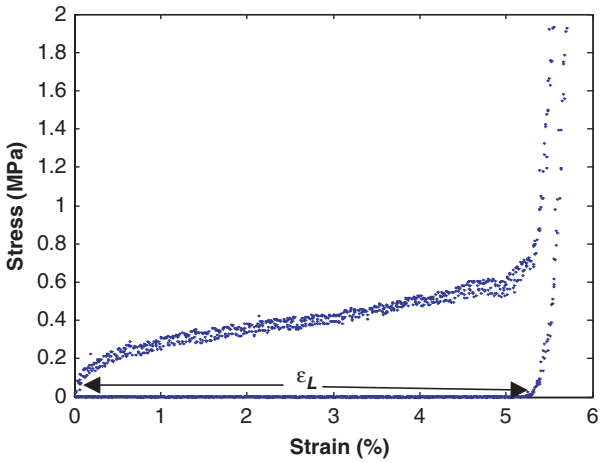

Figure 9. Stress–strain behavior of NiMnGa for zero applied field.

the analytical model will over-predict the critical stresses for large external fields close to saturation ($H_{external} > 7$ kOe). Figure 11 demonstrates this limitation by comparing the model to the experimental stress–strain curve for an 8 kOe external field. The four critical stresses in the predicted stress–strain curve are significantly higher than the actual material behavior. Clearly, the model does not accurately capture the physical behavior of the material in this case. Furthermore, the model is not yet developed enough to capture two important behaviors involving intermediate states: partial pseudoelastic recovery for actuation at fields between H_s and H_f, and minor hysteretic loops. Figure 12(a) shows the experimental data regarding partial pseudoelastic recovery for the case of a 2.5 kOe external field while Figure 12(b) shows the minor hysteretic loops for NiMnGa actuation at a 6 kOe applied field. Further refinements of the model are needed to resolve these issues.

CONCLUSIONS

A simple constitutive model for quasi-static NiMnGa behavior was proposed and developed. Nine parameters

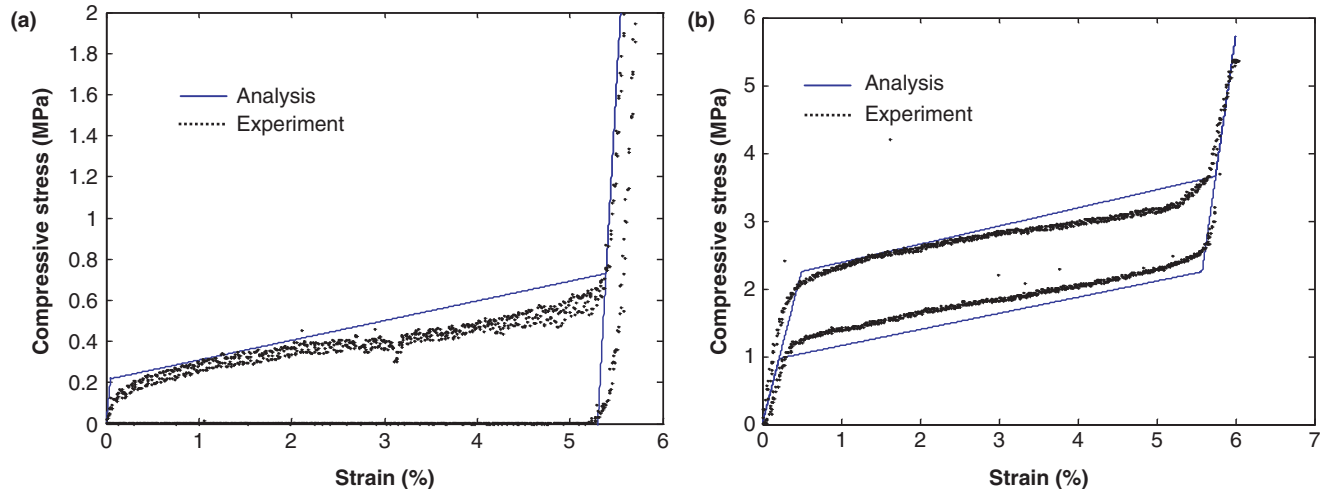

Figure 10. *FSMA model validation: (a) magnetic SME at 0 kOe and (b) magnetic pseudoelasticity at 6 kOe.*

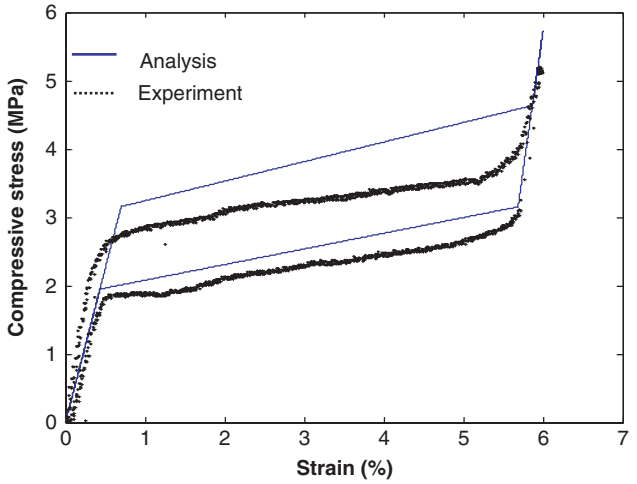

Figure 11. *Comparison of the FSMA model to experimental data for an 8 kOe external field.*

derived from experimental data were identified to fully characterize the model. To obtain these constants, two types of tests were conducted on the NiMnGa rods; one type in which the applied field is varied at a constant stress and another type where the stress was varied in a constant external field. These tests were aimed at measuring the strain and load response of the material for different magnetic and mechanical loading conditions. It was determined that all nine model parameters can be most reliably obtained from the constant external field tests. The parameters include two Young's moduli E_σ, E_H, two fundamental critical threshold fields, H_s, H_f, and a free strain, ε_L. The final four parameters include two fundamental critical stresses, $\sigma_{cr,s}$, $\sigma_{cr,f}$, and two stress influence coefficients, C_s and C_f. The stress influence coefficients and threshold fields were identified from the critical stress versus external field profile, assembled from compression tests in which the material was subjected to a wide range of constant external fields.

Once the material parameters were determined, the model was implemented and compared to test data. The model captures both the MSME and pseudoelastic behavior of the NiMnGa. Although a good correlation exists between the calculated results and the test data, there are several issues that must be addressed in order to improve the accuracy of the model. Because the model is assumed to be both linear and of constant material parameters, it does not accurately capture the smooth transitions of the stress–strain behavior at the beginning and end of twin boundary motion. Also, the linear assumption does not reflect the influence of magnetic saturation, leading to an overprediction of stress at higher applied fields. Despite its inherent limitations, the model captures the fundamental strain recovery mechanisms of NiMnGa and therefore provides a basis for future FSMA analytical models.

FUTURE WORK

The development of a comprehensive behavioral model for NiMnGa is currently underway and further tests are required before the model is validated satisfactorily. In particular, more constant field tests are required to provide a larger data base for validation. A more accurate function describing the transformation from stress- to field-preferred martensite that includes higher-order effects such as magnetic saturation is required to accurately predict the behavior of the NiMnGa. Finally, the quasi-static model will be extended to capture the dynamic behavior of the FSMA and used to develop smart actuators for aerospace applications.

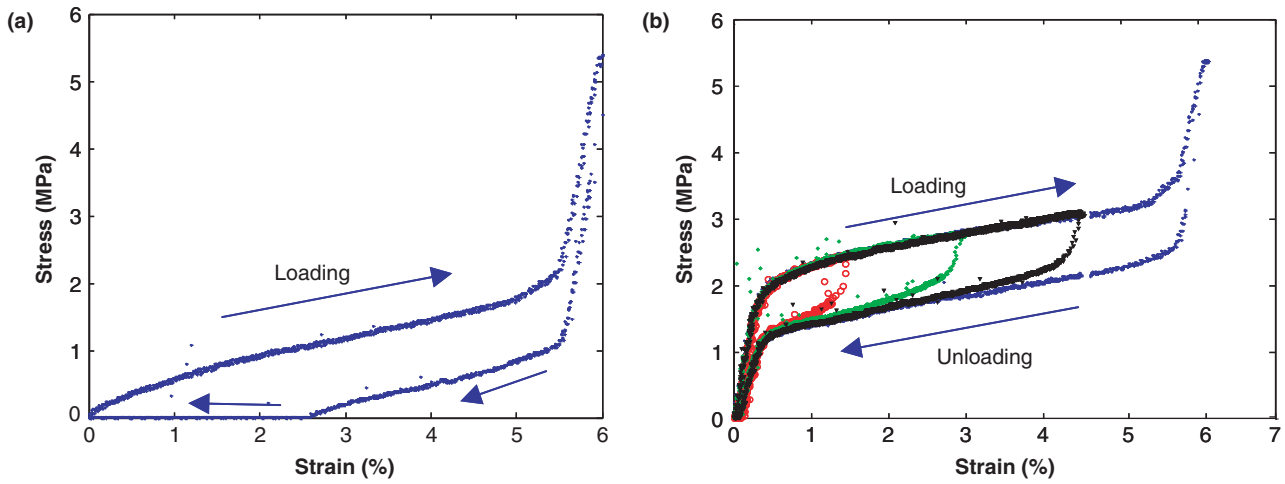

Figure 12. *Intermediate behavior of NiMnGa FSMA: (a) partial pseudoelasticity at 25 kOe and (b) minor hysteretic loops at 6 kOe.*

ACKNOWLEDGMENTS

The research presented in this article is supported by a grant from the Army Research Office with Dr Gary Anderson serving as program monitor through the sponsorship of DARPA under a program with Dr John Main serving as program manager. The authors would also like to thank Mr. Howie Grossenbacher for his technical assistance.

REFERENCES

Adaptamat, Helsinki, Finland.

Brinson, L.C. 1993. "One-dimensional Constitutive Behavior of Shape Memory Alloys: Thermomechanical Derivation with Non-constant Material Functions and Redefined Martensite Internal Variable," *Journal of Intelligent Material Systems and Structures*, 4:229–242.

Cheng, L., Farrell, S. et. al. 2004. "The Influence of Composition and Thermomechanical Treatments on the Magnetic Shape Memory Effect of Ni-Mn-Ga Single Crystals," In: *Proceedings of SPIE*, 5387:137–146, March 2004.

Couch, R. and Chopra I. 2003 "Experimental Characterization of NiMnGa Ferromagnetic Shape Memory Alloy Rods Under Dynamic Magnetic Fields," In: *Proceedings of SPIE*, San Diego.

Likhachev, A., Sozinov, A. and Ullakko, K. 2004. "Magnetic Forces Controlling Magnetic Shape Memory in Ni-Mn-Ga and Their Practical Measurement from the Mechanical Testing Experiments in Constant Magnetic Fields." In: *Proceedings of SPIE*, 5387:128–136, March 2004.

Likhachev, A. and Ullakko, K. 2000. "Magnetic-field-controlled Twin Boundaries Motion and Giant Magneto-mechanical Effects in Ni-Mn-Ga Shape Memory Alloy," *Physics Letters A*, 275:142–151.

Marioni, M., Bono, D. et. al. 2002. "Pulsed Magnetic Field Actuation of Single Crystalline Ferromagnetic Shape Memory Alloy Ni-Mn-Ga," In: *Proceedings of SPIE*, 4699:191–194. March 2002.

Mullner, P., Chernenko, V.A., et al. 2002. "Large Cyclic Deformation of a Ni-Mn-Ga Shape Memory Alloy Induced by Magnetic Fields," *Journal of Applied Physics*, 92(11):6708–6713.

Mullner, P., Chernenko, V.A. and Korstorz, G. 2003. "Stress-Induced Twin Rearrangement Resulting in Change of Magnetization in a NiMnGa Ferromagnetic Martensite," *Scripta Materialia*, 49:129–133.

Murray, S.J. 2001. "Model for Discontinuous Actuation of Ferromagnetic Shape Memory Alloy under Stress," *Journal of Applied Physics*, 89(2):1295–1301.

O'Handley, R.C. 1998. "Model for Strain and Magnetization in Magnetic Shape Memory Alloys," *Journal of Applied Physics*, 83(6):3263–3270.

Prahlad, H. and Chopra, I. 2001. "Experimental Characterization of NiTi Shape Memory Alloy Wires under Uniaxial Loading Conditions," *Journal of Intelligent Material Systems and Structures*, 11(4):272–282.

Rogers, C.A. and Liang, C. 1990. "One-dimensional Thermomechanical Constitutive Relations for Shape Memory Material," *Journal of Intelligent Materials and Structures*, 1:207–234.

Sovinov, A., Likhachev, A., Lanska, N., Ullakko, K. and Lindroos, V. 2002. "Crystal Structure, Magnetic Anisotropy and Mechanical Properties of Seven-Layered Martensite in NiMnGa," In: *Proceedings of SPIE*, 4699:195–205.

Tanaka, K. 1986. "A Thermo-mechanical Sketch of Shape Memory Effect: One-dimensional Tensile Behavior," *Res. Mechanica*, 18:251–263.

Tellinen, J., Soursa, I. et al. 2002. "Basic Properties of Magnetic Shape Memory Actuators," In: *Proceedings of the 8th International Conference ACTUATOR 2002*, Bremen, Germany, June 2002.

Ulakko, K., Likhachev, A. et al. 2000. "Magnetic Shape Memory (MSM) – A New Way to Generate Motion in Electormechanical Devices," *ICEM 2000*, 1195–1199.

Ullakko, K., Huang, J.K., Kantner, C., O'Handley, R.C. and Kokorin, V.V. 1996. "Large Magnetic-field-induced Strains in Ni_2MnGa Single Crystals," *Applied Physics Letters*, 69(13):1966–1968.